

Research Article pubs.acs.org/synthbio

Synthetic Virus-like Particles for Glutathione Biosynthesis

Yang Wang, Masaki Uchida, Hitesh Kumar Waghwani, and Trevor Douglas*



Cite This: ACS Synth. Biol. 2020, 9, 3298-3310



ACCESS I

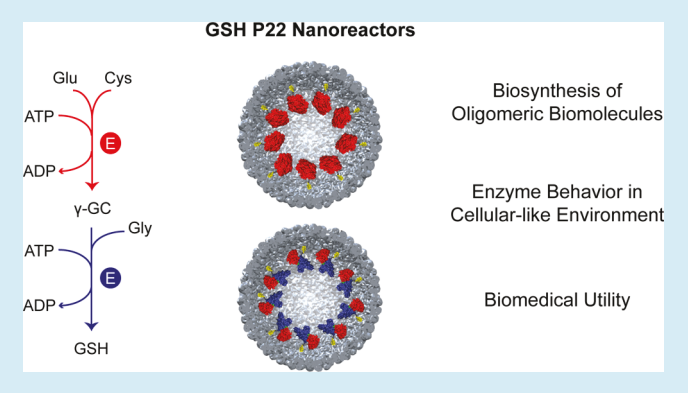
Metrics & More



Article Recommendations

Supporting Information

ABSTRACT: Protein-based nanocompartments found in nature have inspired the development of functional nanomaterials for a range of applications including delivery of catalytic activities with therapeutic effects. As glutathione (GSH) plays a vital role in metabolic adaptation and many diseases are associated with its deficiency, supplementation of GSH biosynthetic activity might be a potential therapeutic when delivered directly to the disease site. Here, we report the successful design and production of active nanoreactors capable of catalyzing the partial or complete pathway for GSH biosynthesis, which was realized by encapsulating essential enzymes of the pathway inside the virus-like particle (VLP) derived from the bacteriophage P22. These nanoreactors are the first examples of nanocages specifically designed for the



biosynthesis of oligomeric biomolecules. A dense packing of enzymes is achieved within the cavities of the nanoreactors, which allows us to study enzyme behavior, in a crowded and confined environment, including enzymatic kinetics and protein stability. In addition, the biomedical utility of the nanoreactors in protection against oxidative stress was confirmed using an in vitro cell culture model. Given that P22 VLP capsid was suggested as a potential liver-tropic nanocarrier in vivo, it will be promising to test the efficacy of these GSH nanoreactors as a novel treatment for GSH-deficient hepatic diseases.

KEYWORDS: virus-like particle, glutathione biosynthesis, therapeutic enzyme delivery, encapsulation, substrate channeling, enzyme protection

ompartmentalization is fundamental to biology and has evolved to control different but specific biological activities in isolated and confined environments. In contrast to compartments surrounded by lipid membranes, compartments assembled from purely proteinaceous material have emerged as an exciting research focus.² There is a large diversity of protein-based compartments with a range of biological functions. Protein compartments that incorporate catalytic species on their interior have evolved as nanoreactors to facilitate specific biochemical activities, separated from the rest of the cell, and play key roles in cellular metabolism.² An advantage for some of these nanoreactors is to enhance the efficiency of the cellular metabolism, which has been demonstrated for the carboxysome found in many cyanobacteria and chemoautotrophs,3 and lumazine synthase in Bacillus subtilis.4 Protein compartments, packaged with various cargos, can also act as nanocarriers for the transport and release of the encapsulated cargo as well as for the storage, sequestration, and protection of the cargo. 5,6 For instance, metastable viral capsids are able to package and release viral genomes through assembly-disassembly pathways, while ferritins are involved in iron homeostasis via mineralization-dissolution of the hydrated iron oxide particle inside the cavity.^{8,9} Studying these protein compartments from nature not only provides insights into fundamental questions in biochemistry, 2-4,10-12 biophysics, 7,13-15 and evolutionary biology, 1,16-18 but also inspires us to design and engineer synthetic nanomaterials, 2,5,6,19,20 and take advantage of both the nanocarrier and nanoreactor properties for applications such as the targeted delivery of catalytic activities with potential therapeutic effects. 20-2

Glutathione (GSH) plays a critical role in metabolic adaptations to chemical challenges in cells.²⁴ As a major endogenous antioxidant molecule, GSH plays a vital role in the liver since one of the main functions of the liver is to detoxify metabolites, including reactive oxygen species (ROS) and strong electrophiles.^{24,25} The normal hepatic level of GSH is about 10 mM, and GSH deficiency can cause liver dysfunction or even conditional lethality.²⁵ Pathological studies indicate that many liver diseases, such as acetaminophen-induced hepatotoxicity, chronic alcoholic disease, and chronic hepatitis C infections, are associated with failure to maintain normal levels of GSH. 25,26 Supplementation with GSH, GSH derivatives, or precursors have been used as effective therapies

Received: July 10, 2020 Published: November 24, 2020





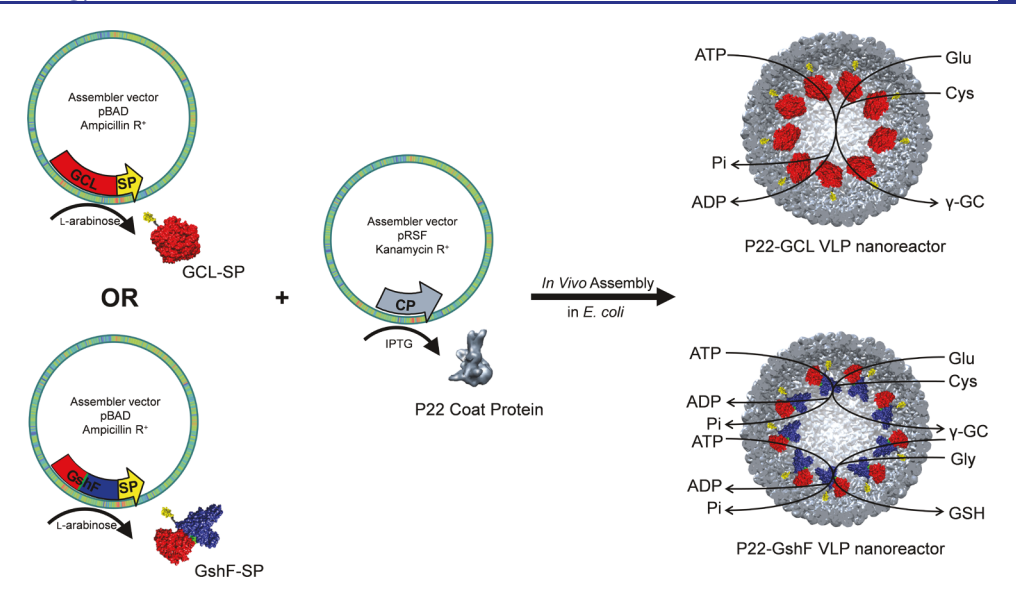


Figure 1. Schematic showing encapsulation of essential enzymes for GSH biosynthesis inside P22 capsid, and the partial or complete GSH biosynthetic pathway catalyzed by the designed nanoreactors. The expression of genes encoding GCL-SP (top) or GshF-SP (bottom) and CP from vectors with different antibiotic resistance (ampicillin and kanamycin) was controlled by different inducers (μ-arabinose and IPTG). The SP (yellow) directed the assembly of CP (gray) and the encapsulation of GCL (PDB: 3IG5) or GshF (PDB: 3LN7) inside P22 capsids in *E. coli*, resulting in P22-GCL or P22-GshF VLP nanoreactors. The linker between GCL (or GshF) and SP, which contains TEV cleavage site, is labeled black. P22-GCL nanoreactor catalyzes the rate-limiting step of GSH biosynthesis by GCL (red), producing γ-GC, the intermediate of the biosynthetic pathway. P22-GshF nanoreactor catalyzes the complete GSH biosynthetic pathway, where γ-GC is synthesized by the GCL domain (red) and GSH is subsequently synthesized by the GS domain (also called ATP-grasp-like domain, blue). The native linker between the two domains of GshF is labeled green. The homodimerization of GshF³⁷ is not shown in this schematic.

at stoichiometrically comparable levels to the amounts of toxic metabolites. 26-28 As an alternative, compensation of GSH biosynthetic activity could circumvent the limitation of stoichiometry as it provides a way to generate GSH in a sustained manner, compared to a single administration of GSH, and an even higher efficacy might be reached if the activity was targeted with in situ production of GSH at the disease sites to prevent off-target effects. A recent study suggests the natural biodistribution of virus-like particles (VLPs) derived from Salmonella typhimurium bacteriophage P22 results in its predominant accumulation in the liver, consistent with previous reports that bacteriophages tend to accumulate in the liver and spleen in vivo. 29-32 This finding inspired us to develop nanoreactors with GSH biosynthetic activities using P22 VLPs, whose natural tropism as nanocarriers could facilitate their delivery to the liver to alleviate GSH deficiency-related hepatic diseases.

P22 VLPs have been shown to be a powerful platform for nanoreactor design and construction. The coat protein (CP) coassembles with scaffolding protein (SP) to form a VLP, which is structurally similar to the prohead of infectious phage that is subsequently loaded with the viral genome.³⁵ Previous studies have shown that truncated SP fused with a cargo protein is still able to direct the programmed selfassembly of the T = 7 icosahedral VLP capsid consisting of 420 CP subunits, while simultaneously achieving guest protein encapsulation. 34,35 By changing the nature of the fusion protein, the VLP can be easily tuned to act as a nanoreactor with different catalytic activities. Thus, the P22 capsid loaded with Escherichia coli hydrogenase 1 is an efficient catalytic material for hydrogen production. 19 In another example, encapsulation of multienzyme cascades within the P22 capsid created a biomimetic metabolic pathway within each nanoreactor. 11 These examples demonstrate that the P22 system is a

mature and robust platform for nanoreactor development. Incorporation of enzymes with therapeutic effects, such as essential enzymes in the GSH biosynthetic pathway, together with the natural tropism of P22 is therefore a goal for the application of this system.

GSH is a nonribosomally synthesized tripeptide produced in a conserved biosynthetic pathway.³⁶ In most species, the pathway requires two ATP-dependent enzymes, glutamate cysteine ligase (GCL) and glutathione synthetase (GS).³⁶ Glutamate cysteine ligase (GCL) synthesizes γ -glutamylcysteine $(\gamma$ -GC) by forming an isopeptide bond between the side chain carboxyl of glutamate and amino group of cysteine, while glutathione synthetase (GS) catalyzes formation of the second peptide bond between glycine and the C-terminus of γ -GC to produce GSH.³⁶ The rate-limiting step of the pathway is γ -GC synthesis, whose rate is regulated by several mechanisms such as GSH feedback inhibition of GCL, post-translational modifications, and holoenzyme formation.³⁶ In contrast, GSH biosynthesis was found to be different in some bacteria, where bifunctional GSH full synthetases (GshFs) have been identified, which possess two catalytic domains with GCL and GS activities, respectively. 36,37 GshFs are less sensitive to GSH feedback inhibition than GCLs,³⁷ suggesting GshFs are good potential candidates for therapeutic biosynthetic purposes. Encapsulation of the critical enzymes of GSH biosynthesis inside the P22 capsid could therefore be used as an approach for making therapeutic nanoreactors.

In this work, we have focused on designing and preparing P22 VLPs with GSH biosynthetic activities and characterizing them from the perspective of synthetic nanoreactors with biomedical potential. Two enzymes were selected as biocatalyst cargos; the monomeric GCL from *Saccharomyces cerevisiae*, which catalyzes the rate-limiting step of GSH biosynthesis,³⁸ and the homodimeric GshF from *Pasteurella*

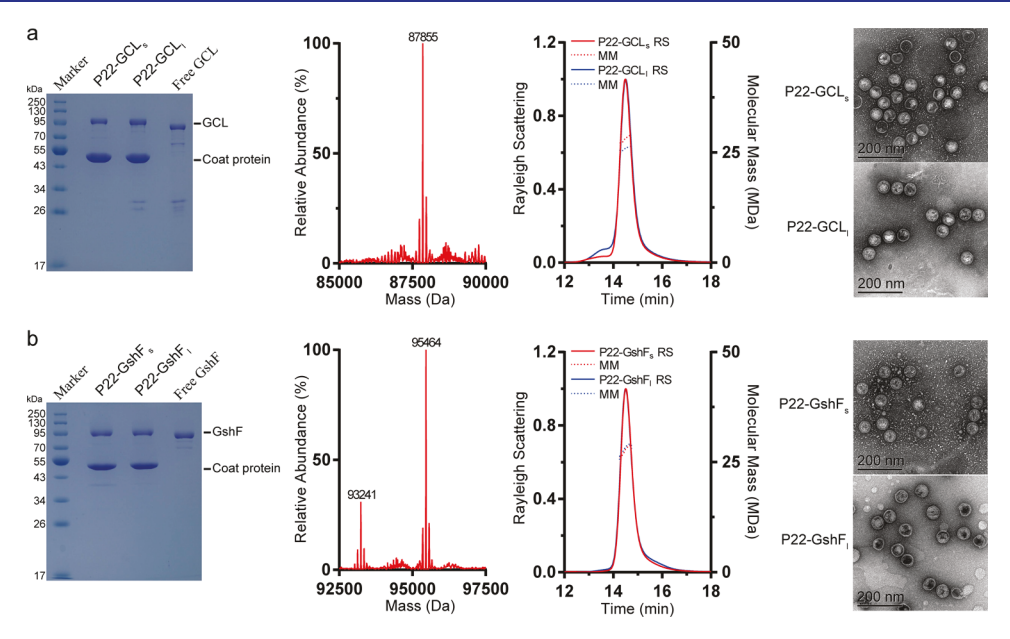


Figure 2. Characterization of P22-GCL and P22-GshF nanoreactors. (a) Characterization of P22-GCL. (b) Characterization of P22-GshF. From left to right: SDS-PAGE shows the approximate molecular weights of the components of the P22 nanoreactors in comparison with free enzymes, and a high purity of the protein samples. LC-MS results indicate GCL-SP (expected 87 856.29 Da) and GshF-SP (expected 95 464.98 Da) remained intact after encapsulation inside P22 capsids, while CP dimer (expected 93 241.34 Da) was also detected. SEC-MALS plots show that the population of P22 nanoreactors are with good monodispersity. TEM images show homogeneity of the nanoreactors.

multocida, which is capable of the complete GSH biosynthesis pathway. 37 Using the SP fusion strategy, where the enzyme was genetically fused to the N-terminus of a truncated SP (amino acid 239-303), multiple copies of these enzymes were encapsulated inside P22 capsids by coexpression and selfassembly with CP. The nanoreactors were catalytically active, being the first example of nanocage-based reactors specifically for the synthesis of oligomeric biomolecules. Additionally, the high copy numbers of enzymes confined in the cavity of P22 capsids creates a crowded environment, with densities of biomacromolecules comparable to the crowded cellular environment. 39,40 Studying the biochemical and biophysical properties of the nanoreactors provides insight into enzyme behavior in crowded conditions from multiple perspectives, such as kinetics, interdomain and intermolecular communications, and stability. Experiments in an in vitro cell culture model explicitly demonstrated protection against oxidative stress with both P22-GCL and P22-GshF nanoreactors. Given the natural tropism of P22 to the liver as a nanocarrier, 21 it will be promising to test the efficacy of the GSH P22 nanoreactors in treating hepatic diseases caused by diminished GSH in liver.

■ RESULTS AND DISCUSSION

Nanoreactor Design and Production. Synthetic nanoreactors able to catalyze the partial or complete glutathione (GSH) biosynthetic pathway were designed and then produced in *E. coli* through the encapsulation of key enzymes inside self-assembled P22 capsids (Figure 1). The enzymes were genetically fused *via* their C-termini to the N-terminus of the truncated scaffolding protein (SP, amino acids 239–303). Two enzymes, *Saccharomyces cerevisiae* glutamate cysteine ligase (GCL) and *Pasteurella multocida* bifunctional glutathione full synthetase (GshF), were used and were separately fused to the SP *via* a linker that contained the TEV protease recognition sequence. Two assembler vectors with different antibiotic resistance and promoters were engineered to

separately harbor the genes encoding GCL-SP (or GshF-SP) and the P22 coat protein (CP), respectively. This allowed us to independently control the expression of the CP and enzyme-SP genes. In one set of experiments, the GCL-SP (or GshF-SP) and CP were simultaneously induced for 5 h by Larabinose and isopropyl β -D-1-thiogalactopyranoside (IPTG), respectively, and the consequent nanoreactors were named P22-GCL_s (or P22-GshF_s). This simultaneous induction strategy is similar to the one vector strategy previously reported, where the CP and cargo-SP fusion were inserted into two multiple cloning sites of one plasmid under control of a single promoter. 10,34 We also used an expression strategy where GCL-SP (or GshF-SP) was induced for 2 h, prior to induction of CP, which was then induced for a further 3 h. This late CP induction for nanoreactor production was termed P22-GCL₁ (or P22-GshF₁). The late CP induction strategy was previously shown to enhance the activity of the nanoreactors, presumably by allowing time to complete enzyme folding and maturation before capsid self-assembly and enzyme encapsulation. 19 The expressed and assembled nanoreactors obtained from E. coli cell lysate were purified by sucrose cushion ultracentrifugation and size-exclusion chromatography prior to their characterization.

Characterization. The self-assembled nanoreactors were comprehensively characterized to determine their biophysical and biochemical properties. Sodium dodecyl sulfate—polyacrylamide gel electrophoresis (SDS-PAGE) analysis showed that all samples were purified to high purity (Figure 2). The migration of each protein fell within the expected molecular weight range, but the encapsulated enzymes showed a slightly higher apparent molecular weight than free enzymes for both GCL-SP and GshF-SP. The subsequent liquid chromatography—mass spectrometry (LC-MS) results (Figure 2 and Figure S1) demonstrated that the encapsulated GCL-SP and GshF-SP both had masses (87 855 and 95 464 Da) that corresponded well to the expected masses (87 856.29 and

Table 1. Property Parameters of P22-GCL and P22-GshF Nanoreactors^a

technique	property parameter	P22-GCL _S	P22-GCL _l	$P22$ - $GshF_S$	P22-GshF ₁	P22 empty shell
LC-MS	enzyme MM (Da)	n.d.	87 855 (expected 87 858.29)	n.d.	95 464 (expected 95 464.98)	N/A
	CP MM (Da)	n.d.	46 623 (expected 46 620.67)	n.d.	46 623 (expected 46 620.67)	46 619.0 ^b (expected 46 620.67)
SEC-MALS	average MM (kDa)	28034.8 ± 33.8	25 975.9 ± 109.7	27731.2 ± 25.7	$28\ 105.2\ \pm\ 15.4$	19025.5 ± 87.5 (expected 19 580.7)
	packing density (enzyme copies per capsid) ^c	102.4 ± 0.4	79.0 ± 1.3	91.1 ± 0.3	95.0 ± 0.2	N/A
	local concentration (mg m L^{-1}) c	321.6 ± 1.3	248.1 ± 4.0	310.9 ± 1.0	324.2 ± 0.6	N/A
	$R_{\rm rms}$ (nm)	23.9 ± 0.8	24.7 ± 0.8	$21\ 8\ \pm\ 0.6$	22.6 ± 0.5	28.3 ± 0.1
	$R_{ m h}$ (nm)	27.0 ± 0.1	26.9 ± 0.1	26.3 ± 0.1	26.7 ± 0.1	26.9 ± 0.1
	$R_{ m rms}/{R_{ m h}}^d$	0.89	0.92	0.83	0.85	1.05
TEM	average diameter (nm)	56.1 ± 1.2	57.8 ± 0.8	55.2 ± 1.0	58.7 ± 1.3	58 ^b

"All data are expressed as mean \pm s.e.m. (n=3) when applicable. n.d. = not determined. N/A = not applicable. ^bData from ref 44. ^cThese parameters are derivatives of average MM of VLPs. ^dThis parameter is a derivative of R_{rms} and R_{h} .

95 464.98 Da, Table 1). The LC-MS also revealed that the purified free GCL-SP and GshF-SP proteins had masses that were 7789-7790 Da lower than the expected molecular weight from the intact proteins (Figure S2). This is likely due to a cleavage at a common site shared between GCL-SP and GshF-SP, and analysis of the LC-MS results and protein sequence suggests that the cleavage occurred between the tyrosine and the phenylalanine residues of the TEV protease recognition sequence (ENLYFQS), a part of the linker connecting the enzyme to the SP. The native cleavage by TEV protease occurs between the glutamine and the serine residues⁴¹ thus it is possible that the cleavage occurred during purification, catalyzed by an endogenous protease from E. coli (see Supporting Information for sequences). The contrast between the susceptibility of the free enzyme to proteolysis and the protection afforded by the capsid to the encapsulated enzymes highlights the role of the physical barrier of the capsid in protection of the encapsulated cargo.

The purified nanoreactors were also analyzed by sizeexclusion chromatography coupled with multiangle light scattering (SEC-MALS, Figure 2). The SEC profiles showed a monodisperse population of particles for all the samples. The particle sizes determined from the angular dependence of the light scattering by MALS and quasi-elastic light scattering (QELS) are summarized in Table 1. Compared to empty P22 capsids, the lower ratios of the root-mean-square charge radius $(R_{\rm rms})$ to hydrodynamic radius $(R_{\rm h})$ of the nanoreactors suggest a dense packing of cargo enzymes. 42,43 The average molecular mass of particles was calculated from MALS data (Table 1) and the experimental average molecular mass of empty P22 capsids was used to calculate the extra molecular mass loaded in the nanoreactors, from which the packing density and local concentration of enzymes inside the capsids were calculated (Table 1), assuming each capsid consists of 420 copies of CP (see Methods). As a comparison, we also determined the enzyme:CP ratio by densitometry analysis of SDS-PAGE gels (see Methods and Figure S3), by which the packing densities and local protein concentration could also be calculated (Table S1). The packing densities are essential in determining the absolute catalytic activities of nanoreactors, which did not vary significantly between the two different methods (see Supplementary Discussion 1). The high local protein concentration, of more than 200 mg mL⁻¹, is similar to the estimated macromolecular concentration in the cellular environment, 39,40 providing us with a good model to study

how the enzymes might behave under confined and crowded conditions as compared to diluted bulk solution conditions.

The morphology of the nanoreactor particles were analyzed by transmission electron microscopy (TEM, Figure 2). The overall population of the nanoreactor particles was homogeneous, with average diameters (Table 1) similar to the procapsid form of P22 VLP (59.6 nm). Most particles were fully assembled and intact, and the size and shape of all four samples were consistent with P22 procapsid morphology. 10,14,34,44

Except that P22-GCL_s has a higher packing density than P22-GCL_b, there is no noticeable difference in the physical properties arising from the two induction strategies (simultaneous induction *versus* late CP induction). Given the interior volume of P22 capsid (46 450 nm³), ¹⁴ and the volumes of GCL (105 nm³) and GshF (116 nm³) that are estimated based on the protein structures, the packing density inside the P22 capsid is calculated to be 18–24% of the available volume, which is similar to the volume occupancy reported previously on the P22 encapsulation system. ^{10,45} These characterization results enabled us to further study the biosynthetic function of these nanoreactors.

Enzymatic Activity and Kinetic Properties. The activity and kinetic properties of each reaction step in the biosynthesis of GSH, catalyzed by the P22 nanoreactors, was measured. These peptide bond-forming reactions consume one molecule of ATP (forming ADP) for each chemical conversion step catalyzed by the enzymes. A coupled pyruvate kinase-lactate dehydrogenase (PK-LDH) assay was utilized to determine the reaction rates by quantitatively connecting the formation of ADP with oxidation of NADH to NAD+, which can be monitored by a decrease in absorption at 340 nm. 46 As each of the synthetic reactions involves three substrates, we measured the kinetic constants for each one independently, while maintaining the other two at saturated (at least 5-times $K_{\rm m}$) conditions in Tris buffer at room temperature. To get the turnover number (k_{cat}) of the reactions for the enzyme, the ratio of initial rate of the reaction to the total enzyme concentration, i.e., $v_0/[E]$, was plotted against substrate concentration, which was then fit to a Michaelis-Menten kinetics model (Figure S4).

The Michaelis constant $(K_{\rm m})$ of both GCL and GshF for the substrates did not change significantly upon encapsulation of the enzyme within P22 capsids; mostly within 20% of the free enzyme (Table 2). The P22 capsid was shown previously to

Table 2. Michaelis-Menten Kinetic Constants Determined by Monitoring ADP Production Using PK-LDH Assay^a

а	Enzyme type	K _m (mM)			k_{cat} (s ⁻¹)		
		Glu	Cys	ATP	Glu	Cys	ATP
	Free GCL	1.84 ± 0.14	5.26 ± 0.48	0.138 ± 0.012	5.24 ± 0.11	5.94 ± 0.16	5.66 ± 0.12
ATP ADP	P22-GCL _s	1.69 ± 0.28	5.12 ± 0.46	0.125 ± 0.016	1.48 ± 0.06	1.63 ± 0.04	1.60 ± 0.05
Glu + Cys GCL/GshF γ-GC	P22-GCL _I	1.72 ± 0.17	4.56 ± 0.27	0.152 ± 0.012	5.05 ± 0.13	5.58 ± 0.10	5.47 ± 0.10
332,33111	Free GshF	5.13 ± 0.75	0.106 ± 0.013	0.341 ± 0.037	15.3 ± 0.8	13.8 ± 0.5	13.0 ± 0.4
	$\mathrm{P22\text{-}GshF}_{\mathrm{s}}$	5.47 ± 0.54	0.140 ± 0.017	0.407 ± 0.026	22.2 ± 0.7	20.9 ± 0.9	19.6 ± 0.4
	P22-GshF _I	5.43 ± 0.91	0.121 ± 0.018	0.398 ± 0.031	19.7 ± 1.1	17.2 ± 0.8	16.1 ± 0.4
b	Enzyme	K _m (mM)			K _{cat} (s ⁻¹)		
ATD ADD	type	Gly	γ-GC	ATP	Gly	γ-GC	ATP
γ -GC + Gly $\xrightarrow{\text{Coh} F}$ GSH	Free GshF	28.4 ± 5.5	0.708 ± 0.143	0.373 ± 0.070	19.3 ± 1.2	19.0 ± 1.5	19.2 ± 1.1
GSIIF	P22-GshF _s	25.9 ± 2.2	0.832 ± 0.061	0.454 ± 0.080	32.2 ± 0.8	35.1 ± 1.1	34.9 ± 2.0

^aAll data are expressed as mean \pm s.e.m. (n = 3). (a) Synthesis of γ-GC from Glu and Cys, the rate-limiting step of GSH biosynthesis, catalyzed by GCL or the GCL domain of GshF. (b) Synthesis of GSH from γ-GC and Gly, catalyzed by GS domain (ATP-grasp-like domain) of GshF.

impose no barrier for the diffusion of small molecules, hence the local concentration of substrates and products inside capsids is essentially the same as that of the bulk solution. Given the free diffusion of substrates, the similar $K_{\rm m}$ values indicate that the affinities between the enzymes and the substrates were not affected by encapsulation.

The turnover number (k_{cat}) of GCL decreased by approximately 70% in P22-GCL_s, but maintained very similar values in P22-GCL, compared to free GCL (Table 2a). It is possible that not all copies of the GCL enzyme inside P22-GCL_s were active, as was reported for other functional proteins encapsulated inside P22 capsids. 10,47 As discussed previously, the time between translation and encapsulation might be insufficient to achieve complete folding and maturation when GCL is simultaneously induced with CP. 19 Alternatively, some copies of encapsulated GCL may undergo denaturation after encapsulation. Another possibility is due to different loading densities, where 20-30 more enzyme copies in average were loaded in P22-GCL_s nanoreactor capsids than P22-GCL_b resulting in an about 30% increase in protein local concentration (Table 1). Some enzymes have been shown to behave differently in crowded environments. 12,48 The decrease in catalytic activities after enzyme encapsulation inside P22 capsids was reported previously, 10,49 with a recent study confirming that the crowded environment of the capsid cavity could influence the enzymatic activity. 12 Therefore, the more crowded local environment of the P22-GCL_s capsids may inhibit enzymatic activity of GCL. Purification of a different batch of the P22-GCL was found to have lower enzyme density (for P22-GCL_s, 67.1 ± 1.4 copies/capsid, i.e., 35.3 copies fewer/capsid; for P22-GCL₁, 68.2 ± 1.1 copies/capsid, i.e., 10.8 copies fewer/capsid), but measurements of the kinetic constants (Table S3) showed comparable results to the old batch of P22-GCL₁ (Table 2a). Thus, the decrease of k_{cat} values for P22-GCLs in the old batch was likely not caused by limited structural maturation during protein production. Instead, the differences between the activity of encapsulated and free GCL might be due to the crowded local environment or protein denaturation inside capsids.

The turnover numbers $(k_{\rm cat})$ of GshF showed a slight increase upon encapsulation. For γ -GC synthesis from Glu and Cys, the $k_{\rm cat}$ values increased about 50% and 25% for P22-

GshF_s and P22-GshF_l, respectively, compared to free GshF (Table 2a). A similar but more distinct trend was also found for GSH synthesis, from γ -GC and Gly, where the k_{cat} values increased about 80% and 50% for P22-GshF_s and P22-GshF_b respectively compared to the free enzymes (Table 2b). These results are somewhat surprising, as many enzymes have been reported to lose some activity after encapsulation because crowding and confinement effects might limit some structural dynamics and necessary conformational changes for catalysis. 10,12,40,48 Structural studies suggests that GshF requires less conformational change upon substrate binding, 50 and therefore its activity might be insensitive to the high-density packing inside the capsid. However, the high local concentration of enzymes, when encapsulated, will drive oligomerization of the enzyme cargo which might be advantageous for multiunit enzymes to enhance enzymatic activities compared to bulk solution, as was reported for Escherichia coli hydrogenase 1.19 Although the two sequential reactions of the GSH biosynthetic pathway can be catalyzed by a single protomer of GshF, intersubunit communication is suggested to influence the function in the dimer of GshF,50 which is expected to be enhanced after encapsulation and may contribute to the slightly increased k_{cat} values observed. The P22-GshF_s showed a slightly higher activity than P22-GshF₁, which again suggests that extra time for enzyme maturation before packaging is not always required to achieve high activity of encapsulated enzymes.

Kinetic Properties of P22-GshF in Catalyzing the Complete GSH Biosynthetic Pathway. Given the high local concentration of the enzymes within the P22 capsids (crowding) we hypothesized that interaction between the two domains and the transport of γ -GC from one active site to the other might be different for the encapsulated GshF from bulk solution environment. Free GshF was reported to show no substrate channeling of γ -GC.³⁷ However, the encapsulation is able to force copies of GshF to pack close to one another, which might provide intermolecular proximity required for channeling. Moreover, the interdomain and intersubunit communications influence the bifunctionality of GshF.⁵⁰ We therefore investigated whether these communications were affected by encapsulation.

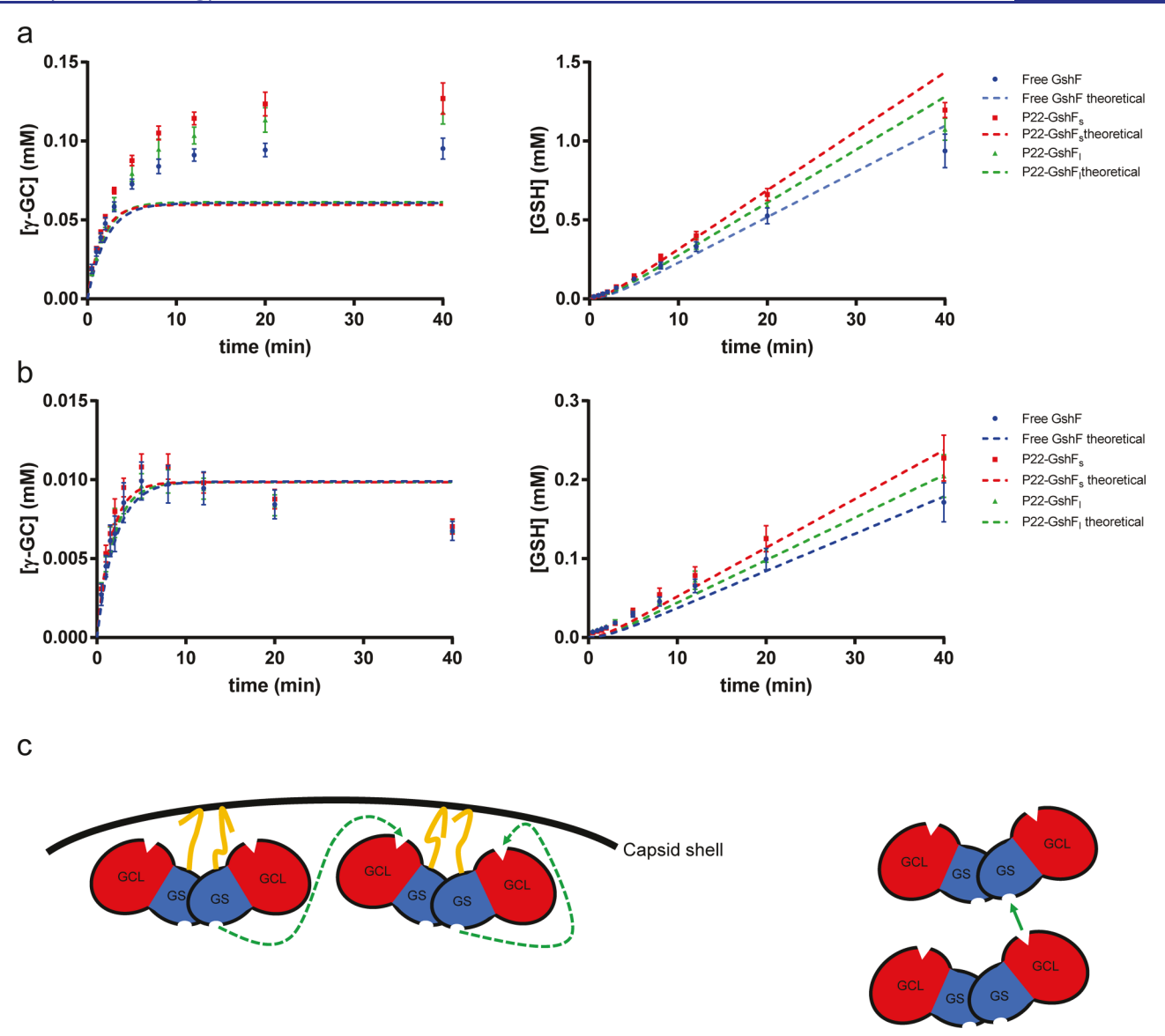


Figure 3. Kinetic study of the GshF-catalyzed complete two-step GSH biosynthetic pathway. (a) Reactions carried out at 50 mM Glu, 2 mM Cys, 350 mM Gly, 5 mM ATP. (b) Reactions carried out at 2 mM Glu, 2 mM Cys, 350 mM Gly, 5 mM ATP. Left: progress plot of γ-GC concentration. Right: progress plot of GSH concentration. All data are expressed as mean \pm s.e.m. (n = 3). The dashed curves represent the theoretical situations where no channeling happens between the two active sites of GshF, calculated from a free diffusion model (see Methods). (c) A cartoon representation of the reaction trajectory catalyzed by P22-GshF (left) and a possible scenario of enzyme packing required by substrate channeling (right). The GCL domain is in red while the GS domain is in blue, and the active sites of the two domains are depicted in different shapes. Encapsulated GshF is likely to be localized to the interior lumen of P22 capsids via the flexible SP (orange) that is fused to the C-termini of GshF protomers. The geometric positions of the domains, the active sites, and fused SP in a GshF dimer have referred to the crystal structure of GshF (PDB: 3LN7). Possible shortest routes of γ-GC in P22 capsids are marked by dashed lines in green (left). A possible substrate channeling event is labeled by a green arrow (right).

The kinetics of the GshF catalyzed reaction for the complete coupled two-step synthesis of glutathione (GSH) were measured using a thiol labeling assay (monobrombimane, mBBr) where the concentrations of both GSH and the intermediate γ -GC were measured. Since the kinetic balance between the two sequential reactions plays an important role in diffusional channeling, we tested the kinetic behavior of GshF under different substrate conditions, where the rate of the first (or second) step was modulated by variable Glu (or Gly) concentrations (Figure 3a and b, Figure S6). To analyze the data, a widely used free diffusion model was applied to predict the accumulation of γ -GC and the production of GSH

under "no channeling" conditions, 52 indicated by dashed lines in the plots.

The accumulation of γ -GC reached a plateau that was higher than predicted in the free diffusion model (Figure 3a left), and a lag in GSH formation was found similar to the free diffusion model (Figure 3a right), when all three amino acid substrates were at saturation. If there was substrate channeling, a lower intermediate concentration at steady state and a faster product formation before steady state should have been observed compared to the free diffusion model. Therefore, these data imply no obvious substrate channeling for either the free or encapsulated GshF when all the substrates are saturated. The kinetic behavior was also analyzed under conditions where

ACS Synthetic Biology Research Article pubs.acs.org/synthbio

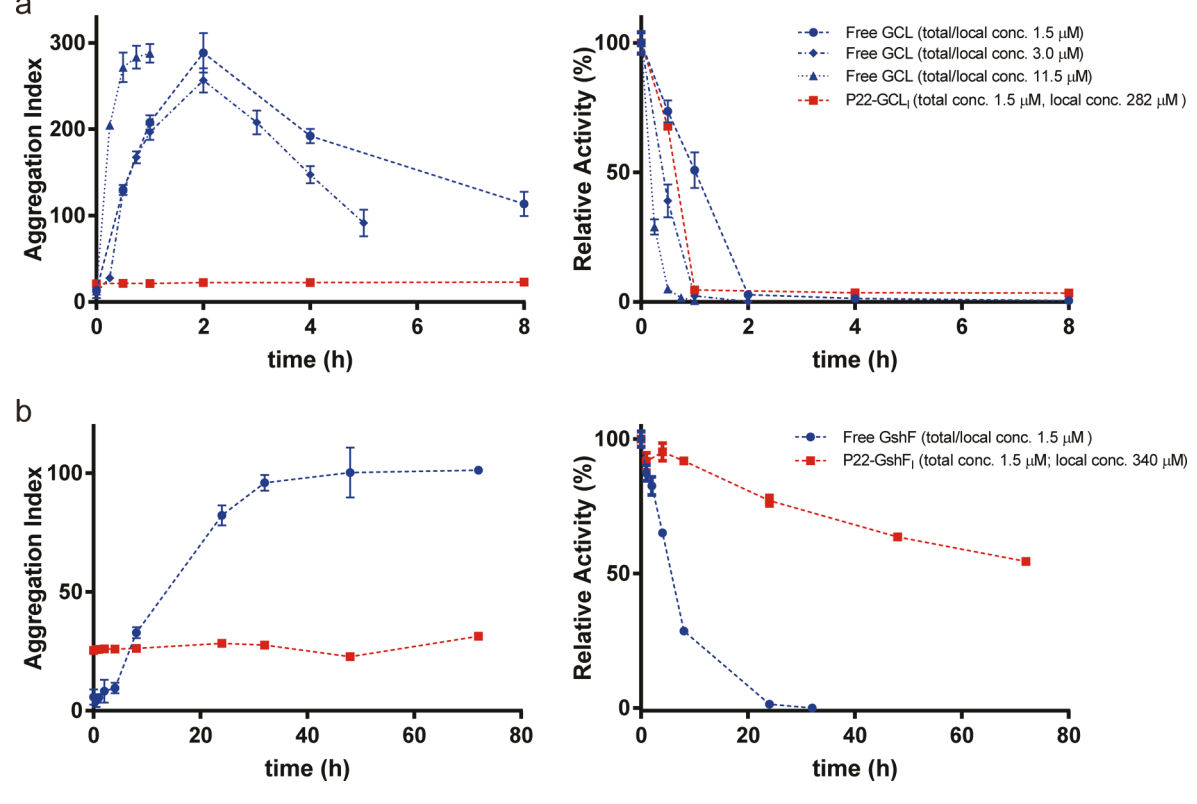


Figure 4. Enzyme thermostability test. (a) GCL. (b) GshF. Left: Progress of aggregation index. Right: Progress of relative activity (%) remained, normalized from the mean at time zero (i.e., 100% activity). The 100% activities (in $v_0/[E]$) were 8.5 s⁻¹ (free GCL at 1.5 μ M), 4.9 s⁻¹ (free GCL at 3 μ M), 3.9 s⁻¹ (free GCL at 11.5 μ M), 6.5 s⁻¹ (P22-GCL₁), 9.8 s⁻¹ (free GshF), and 7.2 s⁻¹ (P22-GshF₁). All data are expressed as mean \pm s.e.m. (n = 3).

[Glu] was under saturated (2 mM, lower than $K_{m,Glu}$ shown in Table 2a) and the first step was slowed so that any leaky channeling should be more obvious. 11 Under these conditions, the accumulation of γ -GC (Figure 3b left) and the production of GSH (Figure 3b right) still fit well into the free diffusion model, and no significant difference was found between the kinetic plots of encapsulated and free GshF. Similar results were also observed under other substrate conditions, including unsaturated [Glu] with concentrations other than 2 mM (15 mM, Figure S6d; and 5 mM, Figure S6e), as well as unsaturated [Gly] (i.e., the first step was kept at maximum rate while the second step was slowed down; Figure S6a-c). Consequently, the intermolecular proximity of GshF enzymes enforced by the encapsulation did not affect the channeling behavior of y-GC between the GCL and GS active sites of GshF.

а

The observed kinetic properties can be understood by considering the geometric configuration of the GCL and GS active sites in a single native dimer of GshF, the packing of GshF dimers in the reported crystal structure, and the possible arrangement of enzyme molecules inside the P22 capsids, as demonstrated by Figure 3c. The lack of any observed channeling in free solution is consistent with the structure of GshF (PDB: 3LN7), which shows that the active sites are not oriented such that the substrate trajectories between them would facilitate channeling as proposed in structure-based models of channeling. ^{37,50} Proximity-induced channeling, enforced by enzyme packing (Figure 3c right), could only realistically be expected to occur when the distances and angles between two adjacent functionally coupled active sites are optimally about 10 Å and 0° (i.e., face to face) as suggested by

a computational study on the requirements for channeling.⁵⁴ However, even in the protein crystals (packing density ~550 mg mL⁻¹) such proximity is not achieved (see Supplementary Discussion 2),50 which allows us to understand the observed absence of substrate channeling in the P22 nanoreactors, which have a lower-density packing of GshF (~300 mg mL⁻¹, Table 1) than in the crystal. In addition, the encapsulated GshF is localized to the interior surface of P22 capsids, ¹⁴ which likely constrains the conformation of GshF so that the required proximity (both distance and orientation) between adjacent GCL and GS active sites is not achieved (Figure 3 left) as demonstrated in our experimental data.

The kinetics of the two-step reaction catalyzed by GshF was also analyzed. The rates of each single step were measured and calculated in the context of the overall coupled two-step GSH synthesis, and plotted as a function of substrate concentration (Figure S7). The high similarity between the kinetic behavior of the free and the encapsulated GshF suggests that encapsulation did not change the dual catalytic behavior of GshF. It is worth noting that, when the GCL activity is at maximum, both the apparent Michaelis constant for Gly $(K_{\rm m,Gly,app})$ and apparent turnover number $(k_{\rm cat,Gly,app})$ of the GS activity (Figure S7d, and Table S5) are significantly lower than the steady-state constants shown in Table 2. This phenomenon is likely due to the fact that the rate of GS activity, the second step of the pathway, is limited by the rate of GCL activity in the context of the coupled reactions.

Thermostability. Many enzymes have been reported to have increased stability after encapsulation within protein capsids. 19,55-57 The stability of GCL and GshF, including protein aggregation and enzymatic efficiency, was measured for

the nanoreactors and free enzymes under physiological temperature conditions (37 °C). Free and encapsulated enzymes in phosphate buffer were incubated at 37 °C, and aliquots were taken at different time points to measure UV-vis spectra to determine the aggregation index (AI) and enzymatic activity of γ -GC synthesis (Figure 4). The AI was used to monitor the formation of aggregates, where an AI value below 10 is generally considered to indicate the presence of no significant aggregates in solution.⁵⁸ P22 capsids with a diameter of about 58 nm show higher light scattering 45 and a slightly higher AI value of about 25 in its normal, monodispersed state. In the free GCL sample no aggregates were detected initially, but aggregates formed very quickly once the sample was incubated at 37 °C, showing a significant increase in AI (Figure 4a left). These aggregates remained dispersed in solution, until they precipitated as visibly insoluble clusters with a relative decrease of the AI. This aggregation behavior matched the change of relative activity of free GCL (Figure 4a right). We did not observe any bulk aggregation for P22-GCL_b, but the enzymatic activity decreased rapidly to about 5% after 1 h and remained at 3-5% activity for another 7 h (Figure 4a). In contrast, GshF showed a much higher thermostability. Free GshF at a concentration of 1.5 μ M only started to aggregate significantly after about 8 h incubation at 37 °C, and the change in activity followed the same trend but did not completely disappear until 24 h (Figure 4b). No visible aggregation was observed in the P22-GshF₁ sample, and more than 50% of the catalytic activity of P22-GshF was retained 72 h after incubation at 37 °C (Figure 4b).

These results show that there is a strong correlation between the increase in AI and the decrease in catalytic activity for free GCL and free GshF, indicating the loss of activity was due to thermally induced aggregation. The P22 nanoreactors, in contrast, had a decrease in activities but an insignificant change in light scattering, suggesting the encapsulated enzymes probably suffered the aggregation induced denaturation inside capsids that was not captured by AI measurements of the bulk solution. Given that an increase in protein concentration tends to cause increased aggregation (Figure S8),⁵⁹ one would expect that enzymes at higher local concentrations should have a higher propensity for aggregation and consequently a faster loss in activity. For GCL, the encapsulated enzyme with a local concentration of 282 μ M (~250 mg mL⁻¹) showed a slower decrease in activity compared to free enzyme at concentrations higher than 3 μ M (0.24 mg mL⁻¹; Figure 4a right), suggesting an enhancement of the enzyme stability upon encapsulation. Similar results were obtained illustrating the stabilization of GshF after encapsulation, where the encapsulated GshF with a local concentration of 340 μ M (~325 mg mL⁻¹) showed slower and less loss of activity compared to free GshF at 1.5 μ M (0.13 mg mL⁻¹; Figure 4b right). This thermal protection effect derived from encapsulation inside P22 capsids has previously been observed in other enzyme constructs, such as hydrogenase and phosphotriesterase. 19,60

To examine whether the encapsulated enzyme could undergo aggregation inside P22 capsids, a SYPRO Orange dye-based thermal shift assay was performed. The intercalation of this dye into the hydrophobic regions of proteins exposed upon thermal denaturation results in enhanced fluorescence, which allows us to visualize the unfolding process of encapsulated proteins inside the thermal-resistant capsids. The data showed that both GCL and GshF were able to unfold inside the capsids but with increased melting temperatures

compared to the free enzymes (Table 3 and Figure S9). These results suggest the potential of protein aggregation inside P22

Table 3. Melting Temperatures of GCL and GshF^a

enzyme	free (°C)	encapsulated (°C)
GCL	40.33 ± 0.06	42.46 ± 0.09
GshF	51.26 ± 0.08	52.97 ± 0.04

^aAll data are expressed as mean \pm s.e.m. (n = 6).

capsids *via* an unfolding pathway, as well as the stabilization effect of the enzymes afforded by encapsulation. This is consistent with a theory proposed by a recent study that thermostability enhancement of enzymes after encapsulation inside protein capsids might be due to the inhibition of protein unfolding.⁵⁷

The phenomenon of the decrease in enzymatic activity of the nanoreactors raises a general issue in enzymology, which is that not all copies of the protein species are necessarily functionally active.⁴⁷ In this study, the activity loss of the enzymes inside P22 capsids could be observed and quantified relative to the initial activity, and rationalized by protein aggregation. Although we are not able to resolve the activity distribution of single enzyme molecules in the encapsulated population (*i.e.*, how active each copy the encapsulated enzymes is), previous results indicate the existence and the variability of partially or completely unreactive species.^{47,62}

In Vitro Cell Protection against Oxidative Stress. The biomedical potential of these nanoreactors capable of catalyzed GSH biosynthesis was examined in cell culture using an in vitro oxidative stress model. Reactive oxygen species (ROS) were induced rapidly by addition of rotenone, a mitochondrial complex I inhibitor, causing oxidative stress in HEK 293FT cells. 63 Different protection strategies were simultaneously applied to cells, and the cell viability was measured 9 h after incubation and normalized to evaluate the effectiveness of protection. All three thiol species in the GSH biosynthetic pathway (Cys, γ-GC, and GSH) were tested as direct ROS scavengers. As shown in Figure 5, Cys provided very little protective effect on the cells, while both γ -GC and GSH showed significant protection. This observation can be understood given that the synthesis of γ -GC is the ratelimiting step of the GSH biosynthesis pathway, 36,64 which might not be rapidly restored after the intracellular redox balance is massively altered. Another two GSH precursors, glutathione monoethyl ester $(GSH-C_2H_5)^{28}$ and \hat{N} -acetylcysteine (NAC),²⁷ also showed nearly the same protective effect as GSH itself. These small molecules, serving as ROS scavengers or scavenger precursors, all combat oxidative stress stoichiometrically. To assess whether cells could be protected from oxidative stress by compensation of the catalytic activity of GSH biosynthesis, 64 the stressed cells were also treated with GCL and GshF, respectively, for their potential to synthesize ROS scavengers. The results suggest that both GCL and GshF showed a significant protective effect against oxidative stress in vitro irrespective of encapsulation even though the enzyme activity was shown to decrease upon incubation at 37 °C (particularly for GCL) in the previous section. Probably, the protective effect of GCL arose from the high activity at the early stage of incubation and the residual activity that remained. Empty P22 capsids were also found to show some nonspecific protective effect, but it is clear from the data that there was an increase in protective efficacy when the enzymes

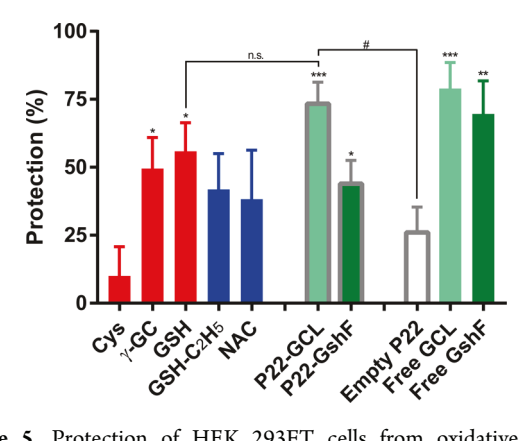


Figure 5. Protection of HEK 293FT cells from oxidative stress. Oxidative stress was induced by rotenone. Reagents added were indicated as molecules within GSH biosynthetic pathway (red), GSH precursors (blue), and GSH makers (light green for GCL, and dark green for GshF). Gray boxes represent P22 capsids for enzyme encapsulation or empty capsids. The protection (%) was measured by cell viability, normalized from the cell viability of normal cells (100%, oxidative stress uninduced) and unprotected cells (0, oxidative stress induced but no protection applied, see Methods). All data are expressed as mean \pm s.e.m. (n = 6). *P < 0.05, *P < 0.01, and **P < 0.01 versus Cys (unpaired P < 0.01, and n.s. P > 0.01 between two indicated groups (one-way analysis of variance test followed by Tukey's multiple comparison test). The data analysis method is described in detail in Supplementary Discussion 3.

for GSH biosynthesis were encapsulated in the P22 capsids, especially GCL.

Delivery of catalytic activity with biomedical efficacy is an emerging therapeutic approach, especially for diseases caused by toxic metabolites which need to be quenched by stoichiometric amounts of antidotes.⁶⁵ GSH is the molecule responsible for maintaining normal intracellular redox potential and neutralizing toxic metabolites, such as ROS, directly and enzymatically.²⁴ P22-GCL and P22-GshF, nanoreactors capable of catalyzing the partial or complete GSH biosynthetic pathway, showed protective effects against oxidative stress in cells, which demonstrates that compensatory GSH biosynthesis is potentially applicable for treatment of diseases caused by GSH deficiency. These results, in combination with the biodistribution property of P22 capsid to the liver, 21 imply that delivery of an enzymatic activity for GSH biosynthesis in vivo using P22 system has great potential to treat hepatic diseases related to GSH deficiency. This therapeutic approach might allow sustained production of GSH in situ at specific disease sites with higher efficacy and lower off-target effects, which could not be achieved by a single administration of GSH that has no targeting behavior and could be cleared quickly from the in vivo environment.

CONCLUSIONS

In this study, we have designed and produced P22 VLP-based nanoreactors that are able to catalyze the partial and complete biosynthesis of GSH by encapsulation of the enzymes in this pathway. The biophysical and biochemical properties of these nanoreactors were comprehensively characterized. To our knowledge, these nanoreactors are the first to accomplish biosynthesis of oligomeric biomolecules and peptide bond formation using nanocage architecture. The nanoreactors provide a biomimetic model to study enzyme behavior in a crowded and confined environment where a local protein

concentration is reached that is as high as the estimated intracellular concentration of biomacromolecules.^{39,40} We performed a series of experiments to study how the catalytic activity and enzyme stability are affected by encapsulation, which gives insight into some fundamental questions in enzymology and protein engineering. By studying the complete two-step GSH biosynthesis of P22-GshF nanoreactors, we found that the high-density packing of GshF in the capsid cavity was neither able to induce diffusional substrate channeling between the two functionally coupled active sites by introducing intermolecular proximity, nor to significantly alter the bifunctionality of the enzyme. Compared to free enzymes, the encapsulated enzymes were spared proteolysis during assembly, purification and storage and much less susceptible to thermal denaturation at high local protein concentrations, demonstrating the protection of the enzyme cargos by P22 VLP capsids. Furthermore, these nanoreactors effectively protect cells against oxidative stress in vitro, suggesting their biomedical potential for enhancing local concentrations of GSH. Given the natural tropism of P22 capsid to the liver *in vivo* as a nanocarrier, ²¹ it will be promising to treat GSH deficiency-caused hepatic diseases by supplementing the GSH biosynthesis using these nanoreactors.

METHODS

Pyruvate Kinase-Lactate Dehydrogenase (PK-LDH) Assay. The reaction was carried out in Reaction Buffer (100 mM Tris, 100 mM NaCl, 20 mM MgCl₂, pH 8.0), containing 0.25 mM NADH (Acros Organics), 2 mM Phosphoenolpyruvic acid tricyclohexylammonium (PEP; Sigma), 7 U mL⁻¹ lactate dehydrogenase (porcine heart, Calbiochem), 7 U mL⁻¹ pyruvate kinase (from rabbit muscle; Leebio), and GCL or GshF (either free or encapsulated; total enzyme concentration [E] ranging from 20 to 200 nM) in a final volume of 120 μ L. To measure kinetics of γ -GC synthesis, the substrates supplemented were L-glutamic acid monosodium (40 mM for GCL and 50 mM for GshF; Alfa Aesar), L-cysteine (40 mM for GCL and 1 mM GshF; Sigma), and ATP disodium (1.5 mM for GCL and 4 mM for GshF; Aldrich). To measure kinetics of GSH synthesis from γ -GC, the substrates supplemented were γ-GC (5 mM; APExBIO), glycine (350 mM, Bio-Rad) and ATP disodium (4 mM). Enzyme was added last to start the reaction. The Agilent Technology Cary 8454 UV-vis was used to monitor absorbance decrease at 340 nm with kinetics mode at 25 $^{\circ}$ C. The slope of the linear part of A_{340} decrease with time was calculated using zero-order mode kinetics in Agilent UV-visible Chem Station, and then corrected from the background A_{340} decrease (reaction mixture without enzyme). The corrected slope was divided by 6220 M⁻¹ cm⁻¹ (extinction coefficient of NADH at 340 nm) to get the initial rate (v_0) of the reaction. This initial rate was divided by total enzyme concentration in the reaction mixture to get $v_0/[E]$, which was then fitted to Michaelis-Menten model for kinetic constants using Prism 7 Version 7.00.

Monobromobimane (mBBr) Labeling Assay. Standard curves for mBBr assay were first made for γ -GC and GSH. The concentration of these thiol species was determined by Ellman's assay. Ellman's assay solution was prepared by dissolving 4 mg 5,5′-Dithio-bis(2-nitrobenzoic acid) (DTNB; Alfa Aesar) in Reaction Buffer. Twenty-five μ L γ -GC or GSH (Alfa Aesar) in reaction buffer with less than 1 mM concentration added to 250 μ L Reaction Buffer in addition of 5 μ L Ellman's assay solution. The mixture was incubated at

room temperature for 15–20 min before measuring A_{412} . The concentration of the thiol species was determined by

$$A_{412} = \varepsilon_{\text{TNB}} c_{\text{thiol}} lD$$

where path length l is 1 cm, $\varepsilon_{\rm TNB}$ is 75 180 M $^{-1}$ cm $^{-1}$, and dilution factor D is $\frac{25\,\mu{\rm L}}{(250+25+5)\,\mu{\rm L}}=\frac{5}{56}$. The thiols with known concentrations were then diluted to make standard thiol solutions. Twenty-five µL standard solution was mixed with 25 uL monobromobimane (mBBr, 6 mM in acetonitrile; Frontier Scientific), and incubated in dark at room temperature for 30-60 min for labeling. The labeling reaction was then quenched by adding 2 μ L methanesulfonic acid (10% in water; ACROS Organics). The species in the sample were separated by Agilent Eclipse XDB-C18 reverse phase column using an Agilent 1100 HPLC system. The elution method was linear gradients with a flow rate of 0.6 mL min⁻¹: 0 min, 81% B; 21.00 min, 86% B; 21.05 min, 0% B; 25.50 min, 0% B; 25.51 min, 81% B; 30.00 min, 81% B; next injection. Solvent A was methanol (J.T. Baker), and solvent B was 0.2% acetic acid (Millipore) in water. The fluorescence signal was measured by Waters 474 Scanning Fluorescence Detector (excitation 380 nm, emission 480 nm, bandwidth 18 nm), and collected by Agilent OpenLAB CDS ChemStation Rev. C.01.07 [27] via Agilent 35900E Dual Channel Interface. Each sample was analyzed twice. The raw chromatogram data were analyzed by Igor Pro 6.37 built-in Gaussian fit to calculate peak area of the labeled thiol species, and the peak area was averaged from the two runs. This whole process was performed in triplicate. The calibration curves were then developed between average peak area and thiol concentration.

The catalytic activity of GshF was determined by this assay. The GSH biosynthesis was conducted in Reaction Buffer, supplemented with either (a) L-glutamic acid monosodium (50 mM), L-cysteine (2 mM), glycine (350 mM), and ATP disodium (5 mM), or (b) γ -GC (variable concentrations), glycine (350 mM), and ATP disodium (5 mM). The reaction was triggered by adding GshF to a final concentration of 50 nM. The reaction was quenched at different time points by aliquoting 25 μ L reaction mixture and mixing it with 25 μ L mBBr (6 mM in acetonitrile), while the labeling also started. Then the labeling mixture was quenched and analyzed while the generated data were processed, in the same way as standard thiol solutions mentioned above. The average peak areas from two HPLC runs were applied into standard curves for γ-GC and GSH to calculate their concentrations. The whole process was performed in triplicate.

The results of GSH synthesis from γ -GC using GshF were fitted to Michaelis—Menten model for kinetics constants using Prism 7 Version 7.00 (Figure S5 and Table S4). Since [γ -GC] decreased during the course of the reaction, the [γ -GC] used for plotting was the average of [γ -GC] at all the time points (1.0, 1.5, 2.0, 2.5, and 3.0 min).

In the complete two-step GSH biosynthesis by GshF, the results were plotted (Figure 3a and b, Figure S6), while the theoretical nonchanneling curves in terms of time t were predicted by a free diffusion model: 52

[GSH] =
$$v_1 t + \left(\frac{v_1}{V_2}\right) K_{m,\gamma-GC} \left(e^{-(V_2 t/K_{m,\gamma-GC})} - 1\right)$$

and

$$[\gamma\text{-GC}] = \nu_1 t - [\text{GSH}]$$
$$= -\left(\frac{\nu_1}{V_2}\right) K_{\text{m},\gamma\text{-GC}} (e^{-(V_2 t/K_{\text{m},\gamma\text{-GC}})} - 1)$$

where v_1 is experimentally measured the first step rate (the rate of the increase in the sum of γ -GC and GSH from 3 to 20 min), $K_{\rm m,\gamma$ -GC} is the Michaelis constant for γ -GC obtained from mBBr labeling assay (Table S4), and V_2 is the maximum rate of the second step with saturated γ -GC and ATP. Note that V_2 varies with different [Gly], and is calculated from [Gly] based on Michaelis—Menten kinetics formula

$$V_2 = \frac{k_{\text{cat},\gamma\text{-GC}}[\text{Gly}]}{K_{\text{m.Gly}} + [\text{Gly}]}[\text{E}]$$

where $k_{\text{cat},\gamma\text{-GC}}$ is the turnover number of the second step from mBBr labeling assay (Table S4), $K_{\text{m,Gly}}$ is the Michaelis constant for Gly obtained from PK-LDH assay (Table 2), and $\lceil E \rceil$ is the total concentration of GshF (50 nM).

Enzyme Thermostability. Free GCL, free GshF, P22-GCL $_{\nu}$ and P22-GshF $_{l}$ in phosphate buffer (50 mM NaPO $_{4}$, 100 mM NaCl, pH 7.0) were incubated at 37 °C. At different time points, an aliquot of protein was taken out from 37 °C, and stored at 4 °C. The UV spectra were measured, and the aggregation index (AI)⁵⁸ were calculated by

$$AI = 100 \times \frac{A_{340}}{A_{280} - A_{340}}$$

The activity of the enzyme was determined by measuring the rate of γ -GC synthesis at a condition with saturated substrates (50 mM Glu, 50 mM Cys, 10 mM ATP) using PK-LDH assay described above. To get the relative activity (%), the obtained $v_0/[E]$ was compared to the average of $v_0/[E]$ at time zero.

In Vitro Cell Protection against Oxidative Stress. A 48well Clear Flat Bottom TC-treated Cell Culture Plate (Falcon, 353078) was incubated with 80 μ L poly lysine (0.1 mg mL⁻¹ in water) at room temperature for more than 30 min, then washed with 200 μ L DPBS (Gibco), and dried under UV light for more than 30 min. The full medium used was DMEM (Gibco) containing 10% fetal bovine serum, 0.1 mM nonessential amino acids (HyClone), 6 mM L-glutamine (HyClone), 1 mM MEM sodium pyruvate (HyClone), 1% Pen-Strep, 0.5 mg mL⁻¹ Geneticin G418 (Teknova). HEK 293FT cells were seeded in the poly lysine-treated 48-well plate at a confluence of 35-40%, and incubated at 37 °C for 27-30 h. Then the medium was replaced by 250 μ L full medium supplemented with 0.25 µL rotenone (100 mM in DMSO; Calbiochem), so that the final concentration of rotenone and DMSO was 100 μ M and 0.1%, respectively. Besides rotenone and DMSO, one of the following potential protective reagents was also supplemented simultaneously (all in final concentrations): 1 mM Cys, 1 mM γ -GC, 1 mM GSH, 1 mM NAC (Alfa Aesar), 1 mM GSH-C₂H₅ (Cayman Chemical), P22-GCL ([CP] = 0.15 mg mL^{-1} and [GCL] = 0.058 mg mL^{-1}), P22-GshF ([CP] = 0.15 mg mL^{-1} and $[GshF] = 0.078 \text{ mg mL}^{-1}$, P22 S39C variant ([CP] = 0.15 mgmL⁻¹), free GCL (0.058 mg mL⁻¹), or GshF (0.078 mg mL⁻¹). Note that DMEM itself contains 0.2 mM Cys and 0.4 mM Gly. P22-GCL, P22-GshF, empty P22, free GCL, and free GshF used here were prepared from ClearColi BL21(DE3) Electrocompetent Cells and free of lipopolysaccharides (see Protein Production section in Supplementary Methods). The control experiments were done with the full medium supplemented with 0.1% DMSO (without oxidative stress), and full medium supplemented with 100 μ M rotenone and 0.1% DMSO (no protection against oxidative stress). Cells were then incubated at 37 °C for 9 h. Then the medium was replaced by 200 μ L Thiazolyl Blue Tetrazolium Bromide (MTT, 0.5 mg mL⁻¹ in DPBS; Biosynth). After another 4 h incubation at 37 °C, MTT was replaced by 250 μ L DMSO to dissolve all the crystals formed, followed by signal reading using Cytation 5 plate reader at 490 nm. Each assay was duplicated in one experiment, and the signals were averaged (S_{490}). The protection (%) was then calculated by

 $\begin{aligned} & \text{Protection (\%)} \\ &= \frac{S_{490, \text{DMSO only}} - S_{490, \text{rotenone plus protective reagents}}}{S_{490, \text{DMSO only}} - S_{490, \text{rotenone only}}} \end{aligned}$

The whole experiment was repeated six times.

ASSOCIATED CONTENT

Supporting Information

The Supporting Information is available free of charge at https://pubs.acs.org/doi/10.1021/acssynbio.0c00368.

Supplementary figures (Figures S1–S9), supplementary tables (Tables S1–S5), supplementary methods (cloning, protein production, protein purification, SDS-PAGE and densitometry analysis, mass spectrometry, determination of protein concentration, SEC-MALS, local protein concentration calculation, TEM, and SYPRO Orange dye-based thermal shift assay), supplementary discussion (methods of determining packing density inside P22 capsids, packing density of GshF in protein crystal, and data analysis of Figure 5), and sequence information (primers, g-blocks, and protein sequences) (PDF)

AUTHOR INFORMATION

Corresponding Author

Trevor Douglas — Department of Chemistry, Indiana University, Bloomington, Indiana 47405, United States; orcid.org/0000-0002-7882-2704; Phone: +1 (812) 856-6936; Email: trevdoug@indiana.edu

Authors

Yang Wang – Department of Chemistry, Indiana University, Bloomington, Indiana 47405, United States

Masaki Uchida — Department of Chemistry and Biochemistry, California State University Fresno, Fresno, California 93740, United States; ocid.org/0000-0003-0710-8834

Hitesh Kumar Waghwani – Department of Chemistry, Indiana University, Bloomington, Indiana 47405, United States

Complete contact information is available at: https://pubs.acs.org/10.1021/acssynbio.0c00368

Notes

The authors declare no competing financial interest.

■ ACKNOWLEDGMENTS

The authors thank Prof. David Giedroc (Indiana University), Physical Biochemistry Instrumentation Facility (Indiana University), and Electron Microscopy Center (Indiana University) for access to their instruments. HEK 293FT cell line is a kind gift of Prof. Charles Dann III (Indiana University). This work was supported in part by grants from the National Science Foundation (NSF-NM CMMI-1922883), the Human Frontier Science Program (HFSP 4124801), and the Indiana Clinical and Translational Sciences Institute funded in part by grant number UL1TR001108 from the National Institutes of Health Center for Advancing Translational Sciences. The content is solely the responsibilities of the authors and does not necessarily represent the official views of the National Institutes of Health.

ABBREVIATIONS

VLP, virus-like particle; GSH, glutathione; γ -GC, γ -glutamylcysteine; GCL, glutamate cysteine ligase; GshF, glutathione full synthetase; CP, P22 coat protein; SP, P22 scaffold protein.

REFERENCES

- (1) Diekmann, Y., and Pereira-Leal, J. B. (2013) Evolution of intracellular compartmentalization. *Biochem. J.* 449, 319–331.
- (2) Frank, S., Lawrence, A. D., Prentice, M. B., and Warren, M. J. (2013) Bacterial microcompartments moving into a synthetic biological world. *J. Biotechnol.* 163, 273–279.
- (3) Hennacy, J. H., and Jonikas, M. C. (2020) Prospects for Engineering Biophysical CO₂ Concentrating Mechanisms into Land Plants to Enhance Yields. *Annu. Rev. Plant Biol.* 71, 461–485.
- (4) Kis, K., and Bacher, A. (1995) Substrate channeling in the lumazine synthase/riboflavin synthase complex of Bacillus subtilis. *J. Biol. Chem.* 270, 16788–16795.
- (5) Aumiller, W. M., Uchida, M., and Douglas, T. (2018) Protein cage assembly across multiple length scales. *Chem. Soc. Rev.* 47, 3433—3469.
- (6) Diaz, D., Care, A., and Sunna, A. (2018) Bioengineering Strategies for Protein-Based Nanoparticles. *Genes* 9, 370.
- (7) Mateu, M. G. (2013) Assembly, stability and dynamics of virus capsids. *Arch. Biochem. Biophys.* 531, 65–79.
- (8) Theil, E. C., Tosha, T., and Behera, R. K. (2016) Solving Biology's Iron Chemistry Problem with Ferritin Protein Nanocages. *Acc. Chem. Res.* 49, 784–791.
- (9) Uchida, M., Kang, S., Reichhardt, C., Harlen, K., and Douglas, T. (2010) The ferritin superfamily: Supramolecular templates for materials synthesis. *Biochim. Biophys. Acta, Gen. Subj.* 1800, 834–845.
- (10) Patterson, D. P., Prevelige, P. E., and Douglas, T. (2012) Nanoreactors by programmed enzyme encapsulation inside the capsid of the bacteriophage P22. *ACS Nano 6*, 5000–5009.
- (11) Patterson, D. P., Schwarz, B., Waters, R. S., Gedeon, T., and Douglas, T. (2014) Encapsulation of an enzyme cascade within the bacteriophage P22 virus-like particle. *ACS Chem. Biol. 9*, 359–365.
- (12) Sharma, J., and Douglas, T. (2020) Tuning the catalytic properties of P22 nanoreactors through compositional control. *Nanoscale 12*, 336–346.
- (13) Comellas-Aragonès, M., Engelkamp, H., Claessen, V. I., Sommerdijk, N. A., Rowan, A. E., Christianen, P. C., Maan, J. C., Verduin, B. J., Cornelissen, J. J., and Nolte, R. J. (2007) A virus-based single-enzyme nanoreactor. *Nat. Nanotechnol.* 2, 635–639.
- (14) Llauró, A., Luque, D., Edwards, E., Trus, B. L., Avera, J., Reguera, D., Douglas, T., Pablo, P. J., and Castón, J. R. (2016) Cargoshell and cargo-cargo couplings govern the mechanics of artificially loaded virus-derived cages. *Nanoscale* 8, 9328–9336.
- (15) Glasgow, J. E., Asensio, M. A., Jakobson, C. M., Francis, M. B., and Tullman-Ercek, D. (2015) Influence of Electrostatics on Small Molecule Flux through a Protein Nanoreactor. *ACS Synth. Biol.* 4, 1011–1019.
- (16) Wörsdörfer, B., Woycechowsky, K. J., and Hilvert, D. (2011) Directed evolution of a protein container. *Science* 331, 589–592.
- (17) Asensio, M. A., Morella, N. M., Jakobson, C. M., Hartman, E. C., Glasgow, J. E., Sankaran, B., Zwart, P. H., and Tullman-Ercek, D.

- (2016) A Selection for Assembly Reveals That a Single Amino Acid Mutant of the Bacteriophage MS2 Coat Protein Forms a Smaller Virus-like Particle. *Nano Lett.* 16, 5944–5950.
- (18) Terasaka, N., Azuma, Y., and Hilvert, D. (2018) Laboratory evolution of virus-like nucleocapsids from nonviral protein cages. *Proc. Natl. Acad. Sci. U. S. A. 115*, 5432–5437.
- (19) Jordan, P. C., Patterson, D. P., Saboda, K. N., Edwards, E. J., Miettinen, H. M., Basu, G., Thielges, M. C., and Douglas, T. (2016) Self-assembling biomolecular catalysts for hydrogen production. *Nat. Chem.* 8, 179–185.
- (20) Jiang, B., Fang, L., Wu, K., Yan, X., and Fan, K. (2020) Ferritins as natural and artificial nanozymes for theranostics. *Theranostics* 10, 687–706.
- (21) Uchida, M., Maier, B., Waghwani, H. K., Selivanovitch, E., Pay, S. L., Avera, J., Yun, E., Sandoval, R. M., Molitoris, B. A., Zollman, A., Douglas, T., and Hato, T. (2019) The archaeal Dps nanocage targets kidney proximal tubules via glomerular filtration. *J. Clin. Invest.* 129, 3941–3951.
- (22) Steinmetz, N. F., Lim, S., and Sainsbury, F. (2020) Protein cages and virus-like particles: from fundamental insight to biomimetic therapeutics. *Biomater. Sci. 8*, 2771–2777.
- (23) Pitek, A. S., Park, J., Wang, Y., Gao, H., Hu, H., Simon, D. I., and Steinmetz, N. F. (2018) Delivery of thrombolytic therapy using rod-shaped plant viral nanoparticles decreases the risk of hemorrhage. *Nanoscale* 10, 16547–16555.
- (24) Deponte, M. (2013) Glutathione catalysis and the reaction mechanisms of glutathione-dependent enzymes. *Biochim. Biophys. Acta, Gen. Subj.* 1830, 3217–3266.
- (25) Yuan, L., and Kaplowitz, N. (2009) Glutathione in liver diseases and hepatotoxicity. *Mol. Aspects Med.* 30, 29-41.
- (26) Townsend, D. M., Tew, K. D., and Tapiero, H. (2003) The importance of glutathione in human disease. *Biomed. Pharmacother*. 57, 145–155.
- (27) Atkuri, K. R., Mantovani, J. J., Herzenberg, L. A., and Herzenberg, L. A. (2007) N-Acetylcysteine–a safe antidote for cysteine/glutathione deficiency. *Curr. Opin. Pharmacol.* 7, 355–359.
- (28) Puri, R. N., and Meister, A. (1983) Transport of glutathione, as gamma-glutamylcysteinylglycyl ester, into liver and kidney. *Proc. Natl. Acad. Sci. U. S. A.* 80, 5258–5260.
- (29) Nungester, W. J., and Watrous, R. M. (1934) Accumulation of Bacteriophage in Spleen and Liver Following Its Intravenous Inoculation. *Exp. Biol. Med.* 31, 901–905.
- (30) Inchley, C. J. (1969) The activity of mouse Kupffer cells following intravenous injection of T4 bacteriophage. *Clin. Exp. Immunol.* 5, 173–187.
- (31) Prasuhn, D. E., Singh, P., Strable, E., Brown, S., Manchester, M., and Finn, M. G. (2008) Plasma clearance of bacteriophage Qbeta particles as a function of surface charge. *J. Am. Chem. Soc.* 130, 1328–1334
- (32) Farkas, M. E., Aanei, I. L., Behrens, C. R., Tong, G. J., Murphy, S. T., O'Neil, J. P., and Francis, M. B. (2013) PET Imaging and biodistribution of chemically modified bacteriophage MS2. *Mol. Pharmaceutics* 10, 69–76.
- (33) Prevelige, P. E., Thomas, D., and King, J. (1988) Scaffolding protein regulates the polymerization of P22 coat subunits into icosahedral shells in vitro. *J. Mol. Biol.* 202, 743–757.
- (34) O'Neil, A., Reichhardt, C., Johnson, B., Prevelige, P. E., and Douglas, T. (2011) Genetically programmed in vivo packaging of protein cargo and its controlled release from bacteriophage P22. *Angew. Chem., Int. Ed.* 50, 7425–7428.
- (35) Reichhardt, C., Uchida, M., O'Neil, A., Li, R., Prevelige, P. E., and Douglas, T. (2011) Templated assembly of organic-inorganic materials using the core shell structure of the P22 bacteriophage. *Chem. Commun. (Cambridge, U. K.)* 47, 6326–6328.
- (36) Franklin, C. C., Backos, D. S., Mohar, I., White, C. C., Forman, H. J., and Kavanagh, T. J. (2009) Structure, function, and post-translational regulation of the catalytic and modifier subunits of glutamate cysteine ligase. *Mol. Aspects Med.* 30, 86–98.

- (37) Vergauwen, B., De Vos, D., and Van Beeumen, J. J. (2006) Characterization of the bifunctional gamma-glutamate-cysteine ligase/glutathione synthetase (GshF) of Pasteurella multocida. *J. Biol. Chem.* 281, 4380–4394.
- (38) Biterova, E. I., and Barycki, J. J. (2010) Structural basis for feedback and pharmacological inhibition of Saccharomyces cerevisiae glutamate cysteine ligase. *J. Biol. Chem.* 285, 14459–14466.
- (39) Rivas, G., Ferrone, F., and Herzfeld, J. (2004) Life in a crowded world. EMBO Rep. 5, 23–27.
- (40) Guin, D., and Gruebele, M. (2019) Weak Chemical Interactions That Drive Protein Evolution: Crowding, Sticking, and Quinary Structure in Folding and Function. *Chem. Rev.* 119, 10691–10717
- (41) Dougherty, W. G., Carrington, J. C., Cary, S. M., and Parks, T. D. (1988) Biochemical and mutational analysis of a plant virus polyprotein cleavage site. *EMBO J. 7*, 1281–1287.
- (42) Hotz, J., and Meier, W. (1998) Vesicle-templated polymer hollow spheres. *Langmuir* 14, 1031–1036.
- (43) Egelhaaf, S. U., and Schurtenberger, P. (1994) Shape transformations in the lecithin-bile salt system: from cylinders to vesicles. *J. Phys. Chem.* 98, 8560–8573.
- (44) Kang, S., Uchida, M., O'Neil, A., Li, R., Prevelige, P. E., and Douglas, T. (2010) Implementation of p22 viral capsids as nanoplatforms. *Biomacromolecules* 11, 2804–2809.
- (45) O'Neil, A., Prevelige, P. E., Basu, G., and Douglas, T. (2012) Coconfinement of fluorescent proteins: spatially enforced communication of GFP and mCherry encapsulated within the P22 capsid. *Biomacromolecules* 13, 3902–3907.
- (46) Belda, F. F., Carmona, F. G., Cánovas, F. G., Gómez, J. C., and Lozano, J. A. (1982) Enzymatic assays: optimization of systems by using pyruvate kinase and lactate dehydrogenase as auxiliary enzymes. *Rev. Esp. Fisiol.* 38, 327–332.
- (47) Sharma, J., Uchida, M., Miettinen, H. M., and Douglas, T. (2017) Modular interior loading and exterior decoration of a virus-like particle. *Nanoscale* 9, 10420–10430.
- (48) Norris, M. G., and Malys, N. (2011) What is the true enzyme kinetics in the biological system? An investigation of macromolecular crowding effect upon enzyme kinetics of glucose-6-phosphate dehydrogenase. *Biochem. Biophys. Res. Commun.* 405, 388–392.
- (49) Sánchez-Sánchez, L., Tapia-Moreno, A., Juarez-Moreno, K., Patterson, D. P., Cadena-Nava, R. D., Douglas, T., and Vazquez-Duhalt, R. (2015) Design of a VLP-nanovehicle for CYP450 enzymatic activity delivery. *J. Nanobiotechnol.* 13, 66.
- (50) Stout, J., De Vos, D., Vergauwen, B., and Savvides, S. N. (2012) Glutathione biosynthesis in bacteria by bifunctional GshF is driven by a modular structure featuring a novel hybrid ATP-grasp fold. *J. Mol. Biol.* 416, 486–494.
- (51) Newton, G. L., Dorian, R., and Fahey, R. C. (1981) Analysis of biological thiols: derivatization with monobromobimane and separation by reverse-phase high-performance liquid chromatography. *Anal. Biochem.* 114, 383–387.
- (52) Meek, T. D., Garvey, E. P., and Santi, D. V. (1985) Purification and characterization of the bifunctional thymidylate synthetase-dihydrofolate reductase from methotrexate-resistant Leishmania tropica. *Biochemistry* 24, 678–686.
- (53) Wheeldon, I., Minteer, S. D., Banta, S., Barton, S. C., Atanassov, P., and Sigman, M. (2016) Substrate channelling as an approach to cascade reactions. *Nat. Chem.* 8, 299–309.
- (54) Bauler, P., Huber, G., Leyh, T., and McCammon, J. A. (2010) Channeling by Proximity: The Catalytic Advantages of Active Site Colocalization Using Brownian Dynamics. *J. Phys. Chem. Lett.* 1, 1332–1335.
- (55) Chakraborti, S., Korpi, A., Kumar, M., Stępień, P., Kostiainen, M. A., and Heddle, J. G. (2019) Three-Dimensional Protein Cage Array Capable of Active Enzyme Capture and Artificial Chaperone Activity. *Nano Lett.* 19, 3918–3924.
- (56) Giessen, T. W., and Silver, P. A. (2016) A Catalytic Nanoreactor Based on in Vivo Encapsulation of Multiple Enzymes

- in an Engineered Protein Nanocompartment. ChemBioChem 17, 1931–1935.
- (57) Das, S., Zhao, L., Elofson, K., and Finn, M. G. (2020) Enzyme Stabilization by Virus-Like Particles. *Biochemistry* 59, 2870–2881.
- (58) Katayama, D. S., Nayar, R., Chou, D. K., Campos, J., Cooper, J., Vander Velde, D. G., Villarete, L., Liu, C. P., and Cornell Manning, M. (2005) Solution behavior of a novel type 1 interferon, interferon-tau. *J. Pharm. Sci.* 94, 2703–2715.
- (59) Wang, W., Nema, S., and Teagarden, D. (2010) Protein aggregation-pathways and influencing factors. *Int. J. Pharm.* 390, 89–99.
- (60) O'Neil, A., Prevelige, P. E., and Douglas, T. (2013) Stabilizing viral nano-reactors for nerve-agent degradation. *Biomater. Sci. 1*, 881–886.
- (61) Huynh, K., and Partch, C. L. (2015) Analysis of protein stability and ligand interactions by thermal shift assay. *Curr. Protoc. Protein Sci.* 79, 28.29.21–28.29.14.
- (62) Fiedler, J. D., Brown, S. D., Lau, J. L., and Finn, M. G. (2010) RNA-directed packaging of enzymes within virus-like particles. *Angew. Chem., Int. Ed.* 49, 9648–9651.
- (63) Chen, Y., McMillan-Ward, E., Kong, J., Israels, S. J., and Gibson, S. B. (2007) Mitochondrial electron-transport-chain inhibitors of complexes I and II induce autophagic cell death mediated by reactive oxygen species. *J. Cell Sci. 120*, 4155–4166.
- (64) Krejsa, C. M., Franklin, C. C., White, C. C., Ledbetter, J. A., Schieven, G. L., and Kavanagh, T. J. (2010) Rapid activation of glutamate cysteine ligase following oxidative stress. *J. Biol. Chem.* 285, 16116–16124.
- (65) Patgiri, A., Skinner, O. S., Miyazaki, Y., Schleifer, G., Marutani, E., Shah, H., Sharma, R., Goodman, R. P., To, T. L., Robert Bao, X., Ichinose, F., Zapol, W. M., and Mootha, V. K. (2020) An engineered enzyme that targets circulating lactate to alleviate intracellular NADH:NAD. *Nat. Biotechnol.* 38, 309–313.
- (66) Riddles, P. W., Blakeley, R. L., and Zerner, B. (1983) Reassessment of Ellman's reagent. *Methods Enzymol.* 91, 49–60.